Metal Amorphous Nanocomposite (MANC) Soft Magnetic Material (SMM) Enabled High Power Density, Rare Earth Free Rotational Machines

Satoru. Simizu,[1] Paul. R. Ohodnicki[2] and Michael. E. McHenry[1]

[1]Department of Materials Science and Engineering, Carnegie Mellon University, Pittsburgh, PA 15213, USA
[2]National Energy Technology Laboratory, Pittsburgh, PA 15236, USA

Abstract

Metal amorphous nanocomposites (MANCs) are promising soft magnetic materials (SMMs) for power electronic applications offering low power loss at high frequency and maintaining a relatively high flux density. While applications in certain motor designs have been recently modeled, their widespread application awaits scaled manufacturing of MANC materials and proliferation of new higher speed motor designs. A hybrid motor design based on permanent magnets and doubly salient stator and rotor is reported here to develop a compact (a factor of 10 smaller than currently possible in Si steels), high speed (>1 kHz, electrical), high power (>2.5 kW) motor by incorporating low loss (<10 W/kg at 1 kHz) MANCs such as recently reported Fe-Ni-based alloys. A feature of this motor design is flux focusing from the permanent magnet allowing use of lower energy permanent magnet chosen from among non-rare earth containing compositions and attractive due to constraints posed by rare earth criticality. A 2-dimensional finite element analysis model reported here indicates that a 2.5 kW hybrid motor may be built with a permanent magnet with a 0.4 T remanence at a rotor speed of 6000 rpm. At a magnetic switching frequency of 1.4 kHz, the core loss may be limited to < 3 W by selecting an appropriate MANC SMM. The projected efficiency exceeds 96 % not including power loss in the controller. Under full load conditions, the flux density distributions for the soft magnetic material stay predominantly < 1.3 T, the saturation magnetization of optimized FeNi-based MANC alloys. The maximum demagnetizing field in the permanent magnet is less than 2.2×10^5 A/m sustainable, for example, with a high grade hard ferrite magnet.

I. Introduction

A breakthrough in the materials development can trigger renewed interest in mature technologies. Metal amorphous nanocomposites (MANC)s are promising soft magnetic materials (SMM)s featuring low power loss at high frequency and maintaining relatively high flux density. A recently reported $(Fe_{70}Ni_{30})_{80}Nb_4Si_2B_{14}$ MANC material has been shown to have a saturation flux density of 1.3 T with power loss of 0.9 W/kg at 1 T and 400 Hz and 2.4 W/kg at 1 T and 1 kHz [1]. MANCs have metastable nanocomposite structures which remain stable to several 100 ^{0}C without danger of deleterious secondary crystallization [2]. FeNi-based compositions are more economical than previously reported Co-based MANC materials[3] that were considered for higher speed motor topologies [4], [5] considering both the substitution for Co and ability to use lower cost ferroboron and ferroniobium raw materials [6]. In contrast to the MANCs, 3 % silicon steel which is commonly used for motor construction incurs about 10 times power loss under the same condition. Availability of such a material would make a motor design feasible even when requiring a large number of poles and a high operating speed.

In high efficiency motors, use of permanent magnets is advantageous. NdFeB magnets have been incorporated in high efficiency, high power density motor designs with great success. However, rare earth criticality, being imposed by resource locations, cost and environmental issues places constraints on over-relying on this resource [7], [8]. A design based on rare earth free low energy permanent magnets is an important consideration for new motor development.

Zhu et al. [9] gives a detailed account of a flux-switching permanent magnet machine with a doubly salient stator and rotor topology. The examined design was for a relatively small 3-phase synchronous control motor with a low mechanical speed (400 W at 400 rpm). The ratio of electrical to mechanical speed is 10:1 and the loss in the soft magnets is a major constraint in running this motor at a high speed. However, the basic topology has a potential to develop into compact, high speed (>1 kHz, electrical), high power (>2.5 kW) motor by incorporating low loss soft magnetic materials. An additional feature of this motor design is focusing of flux from the permanent magnet which allows the use of lower energy permanent magnets that can be chosen from among non-rare earth containing compositions. Here, we examine the feasibility of such an approach by finite element analysis (FEA) and address other technical challenges.

II. Power Loss Estimation

Power loss generated in SMMs under periodically changing magnetomotive force may be approximated by Steinmetz equation $kf^{\alpha}B^{\beta}$ where f is the frequency, B is the peak flux density, and k a constant [10]. To fit the data over a wide range, the equation is expanded by decomposing loss components into hysteretic, classical eddy current, and excess losses. The power indices α and β were set to 2 for eddy current and 1.5 for excess loss. The same method was applied to available Si-steel data to arrive at parameters summarized in Table I. These equations were used to estimate the power loss from the calculated flux density distribution.

Table I HERE

III. Motor Topology

Zhu et al. examined the case where the number of stator slots (N_S) is 12 and the number of rotor poles (N_R) is 10 (Fig. 1(a)) [9]. Twelve coils are wound without overlap sharing the slot with the adjacent coil and organized into 3 phases. Figure 1(b) shows the flux-linkage (zero current) for each of four coils (A1~A4) in the same phase as the rotor makes a 36-degree turn that corresponds to one full electrical cycle. The profile of one pair (A1 and A3) is exactly matched due to symmetry with a close match with another pair (A2 and A4). The combined induced voltage profile for each phase that consists of four coils is nearly sinusoidal and the motor may be driven as a synchronous three-phase motor.

FIG.1a HERE

FIG.1b HERE

Since torque is proportional to the number of rotor poles, it appears advantageous to increase it as much as possible within manufacturing constraints until it incurs too much power loss or the reduction in flux linkage negates the gain by an increase in pole number. However, it should be noted that parameters N_S and N_R may not be freely chosen. For example, in the case of N_S=12, if one increases N_R from 10 to 11, the flux-linkage for the four coils no longer closely match. Instead, the profile for each coil is phase-shifted by 90° as shown in Fig. 2(a). This peculiar behavior can be understood by examining the phase relationship of the stator coils. As schematically shown in Fig. 2(b), each of the coils goes through one full electrical cycle as the rotor makes a mechanical rotation of $360/N_R$ degrees. Therefore, Coil B1, which is located $360/N_S$ degrees away from Coil A1 experiences a delay of $360N_R/N_S$ degrees in addition to 180° phase shift due to the polarity difference in the associated permanent magnet.

FIG.2a HERE

FIG.2b HERE

In general, the phase relationship of flux linkage profile can be expressed as:

$$\text{Phase difference (in degree)} = \text{mod}(180*\text{mod}(n,2)-n*(N_R/N_S)*360, 360) \quad (1)$$

where n is an integer consecutively numbered for individual coils with the reference coil as 0. Function mod is a modulo operator and mod(n,2) is unity for odd and zero for even numbers. This term accounts for alternating polarity of the associated magnet for the adjacent coils.

The phase relationship of the coils with choices of N_S and N_R is explored in Table II. The phases of intra-phase coils (A1 ~ A4) must match and inter-phase coils (A1, B1, C1) must be shifted by 120°. Not all combinations of N_S and N_R match, as summarized in Table II. E.g., if 12

slots are selected for the stator with four coils, one cannot select N_R=11 because the phases for the four coils in the same phase (A1 ~ A4) do not align. In addition, the relationship with the coils in other phases (B and C) does not exhibit a 120° phase shift required for 3-phase operation. (The phase of an individual coil may be changed by 180° by changing the connection polarity. But, in this case, such changes do not correct the problem.) Another condition for selection is that for smooth switching of flux, the number N_S and N_R should not be too dissimilar.

TABLE II HERE

IV. Design Parameters and Performance

Finite element analysis was performed using COMSOL Multiphysics analysis package with its AC/DC module. The three-phase coil current was set to be sinusoidal and the resultant toque was calculated with Arkkio's method[11] integrating rB_rB_ϕ/μ_0 over the air gap area. Here, B_r and B_ϕ are the radial and tangential component of the flux density, respectively and *r* is the radial positional coordinate. The finite element meshes were refined until the results were consistent within 0.1 %. The results were checked against two additional methods. The induced voltage in the coil was calculated from the electric field that is derived from the time derivative of the vector potential. It was also calculated by taking a time derivative of the flux that threads the coil. The power and thus the torque was calculated by multiplying the current. All three methods gave closely matched results as summarized in Table III.

TABLE III HERE

The torque was calculated for four valid cases listed in Table II for N_R=8, 10, 14, and 16 while keeping N_S at 12. As shown in Fig. 3, 14-pole rotor gives the highest torque with low ripple and thus this was selected for further investigation. The performance is much degraded when N_R= 8 or 16.

FIG.3 HERE

Zhu et al. found that the torque is highest when the ratio of rotor radius to stator outer radius is 0.55 ~ 0.6.[9] In the present work, this ratio was set to 0.59 and the motor radius and active length was selected to achieve 2.5 kW of power at a speed of 6000 rpm. Main design parameters and performance data based on this choice are given in Table IV. The motor's

power reaches 2.6 kW with a torque of 4.13 Nm at a mechanical rotational speed of 100 Hz (6000 rpm). The electrical speed is 1.4 kHz because the number of the rotor poles was set to 14.

TABLE IV HERE

The 3-phase current is 12 A for the 24-turn coil and corresponds to 6.4 A/mm^2. The coil joule heating loss is 29 watts. At 1.4 kHz, the loss in the soft magnetic cores can be quite high if 3% silicon steel is employed. With the equations shown in Table I, it will amount to 93 W. In contrast, the FeNi MANCs exhibit a 30-fold reduction to only 2.8 W of loss. The combined core and joule heating loss of 32 W amounts to just 1.2 % of the output power when the FeNi MANC is adopted. Assuming natural convective air cooling at a rate of 10 W/Km^2, the motor's ultimate temperature rise will be ~60 °C. The actual power loss will be higher when frictional loss is accounted for perhaps reaching 3-4 %, but further temperature rise can be limited by usual means of cooling such as heat sinks and air flow.

FIG. 4a HERE

FIG. 4b HERE

Fig. 4 shows the distribution of the flux density in the soft-magnetic components. No saturation effect is considered in these calculations. When no currents are applied (no load), the flux density is within the expected saturation limit (1.3 T) of FeNi MANCs. Under a full load condition, a small fraction the soft-magnetic components experience the flux density in excess of 1.4 T. This needs to be carefully examined when more definitive data become available for the candidate MANC material. However, the saturation problem may be mitigated by minor geometrical modifications and selection of the permanent magnet remanence.

Because of the flux focusing, the magnetizing field inside the permanent magnets remains relatively small even when the gap flux density amounts to 1-1.1 T. The magnetizing field was calculated with the remanence set at 0.4 T and the recoil permeability to 1. The distribution is shown in Fig. 5 for no load (I=0 A) and full load (I=12 A) conditions. The maximum demagnetizing field is about 2.2 x 10^5 A/m (2.4 kOe). Presently available ferrite permanent magnets show remanence of 0.4 T and coercivity of 2.5 kOe at room temperature. However, the reduction in remanence at elevated temperatures would degrade the performance. Unlike most other permanent magnets, the coercivity increases at elevated temperatures. MANC misrostructures are also notably stable at elevated temperatures in both Co-based [12] and FeNi-based [2] systems. Small improvements in permanent magnet properties are beneficial to motor development [13]. Magnets based on abundant rare earths, e.g. Ce, may be of future interest [14].

FIG. 5a HERE

FIG. 5b HERE

V. Axial Motor

Since the available forms of MANCs are currently limited to ribbons of a certain width, a design that requires stamping out a large area does not yet appear to be feasible. An axial topology is more suitable to overcome this limitation. For this reason, an axial motor model was also considered. The axial motor poses a challenge in FEA modelling because the problem needs to be solved as a 3-d model. In the radial design, the basic performance can be calculated in a 2-d model because we can assume that the flux linkage pattern holds along the rotational axis except for the fringing effect on both ends of the motor. In the axial design, such a symmetry is absent. We have developed 3-d axial motor models and initiated optimization study. The results will be reported separately.

VI. Conclusions

A motor design that combines permanent magnets and a salient rotor structure has been examined incorporating low loss soft magnetic material. A simulation based on 2-d finite element method show the motor designed with permanent magnets of 0.4 T remanence produces an output power of 2.6 kW when running at 6000 rpm (100 Hz) and magnetic switching rate of 1400 Hz. By employing a Fe-Ni based MANCs material, the core loss will be less that 3 W at the rated power. In contrast, with the Si steel, the incurred core loss will exceed 90 W making the design nearly infeasible. Because of the flux focusing design, the permanent magnets may be selected from ferrite magnets rather than high energy rare earth permanent magnets.

Acknowledgment

The authors acknowledge support from the DOE AMO program through DOE/EERE – Office of Advanced Manufacturing Program Award Number: DE-EE0007867.

References

[1] N. Aronhime, V. DeGeorge, V. Keylin, P. Ohodnicki, and M. E. McHenry, "The Effects of Strain-Annealing on Tuning Permeability and Lowering Losses in Fe-Ni based Metal Amorphous Nanocomposites. " J. Materials, in press, (2017).

[2] N. Aronhime, E. Zhoglin, V. Keylin, X. Jin, P. Ohodnicki, and M. E. McHenry, "Magnetic Properties and Crystallization. Kinetics of $(Fe_{100-x}Ni_x)_{80}Nb_4Si_2B_{14}$ Metal Amorphous Nanocomposites." Scripta Mat. 120C, 133-137, (2017).

[3] A. Leary, V. Keylin, A. Devaraj, V. DeGeorge, and P. Ohodnicki and M. E. McHenry; "Stress Induced Anisotropy in Co-rich Magnetic Nanocomposites for Inductive Applications." J. Mat. Res. **31** (20), 3089-3107, (2016) Editor's Feature.

[4] J. M. Silveyra, A. M. Leary, V. DeGeorge, S. Simizu, M. E. McHenry, High Speed Electric Motors Based on High Performance Novel Soft Magnets. J. Appl. Phys. **115**, 17A319-21, (2014). (http://dx.doi.org/10.1063/1.4864247).

[5] J. Silveyra, P.Xu, V. Keylin, V. DeGeorge, A. Leary, "Amorphous and Nanocomposite Materials for Energy-efficient Electric Motors," J. Elec. Mat. **45**, 219-25 (2016).
[6] M. Kurniawan, V. Keylin and M. E. McHenry, "Alloy Substituents for Cost Reduction in Soft Magnetic Materials," J. Mat. Res. **30(8),** 1072-77 (2015). http://dx.doi.org/10.1557/jmr.2015.56.
[7] N. Carsen, R. Fingers, M. E. McHenry, D. Chaumette, L. Alger, "Risks to the Rare Earth Elements Supply Chain." NATO Report Unclassified (2015).
[8] J. D. Widmer, R. Matrin, M. Kimiabeigi, "Electric Vehicle Traction Motors without Rare Earth Magnets," Sustainable Mate rials and Technologies **3**, 7 (2015).
[9] Z. Q. Zhu., Y. Pang, D. Howe, S. Iwasaki, R. Doedhar, and A. Pride, "Analysis of Electromagnetic Performance of Flux-Switching Permanent Magnet Machines by Nonlinear Adaptive Lumped Parameter Magnetic Circuit Model," IEEE Tans. MAG **41**(11), 4277-4287 (2005).
[10] C.P. Steinmetz, Am. Inst. Electr. Eng. Trans. **3**, 3 (1892).
[11] A. Arkkio, Acta Polytechnica Scandinavica, 1987, p56.
[12] V. Degeorge, E. Zoghlin, V. Keylin, and M. McHenry, "Time temperature transformation diagram for secondary crystal products of Co-based Co-Fe-B-Si-Nb-Mn soft magnetic nanocomposite," J. Appl. Phys., **117**, 17A329 (2015).
[13] H, Taguchi, T. Takeishi, K. Suwa, K. Masuzawa, and Y. Minachi, "High Energy Ferrite Magnets," Journal de Physique IV Colloque, **07 (C1)** C1-311 (1997).
[14] S. Takata, "Permanent Magnet Properties and Microstructures of Chill-Cast (Ce-MM)-Cu-Co Ternary Alloys," J. Japan Inst. Metals, **37**, 222 (1973); Trans. JIM 14, 477 (1973).

Table I
Steinmetz parameters for power loss estimates

Material	Hysteresis			Eddy current			Excess		
	k(W/kg)	α	β	k(W/kg)	α	β	k(W/kg)	α	β
Si-steel	51.7	1.0	1.83	20.8	2.0	2.0	14.15	1.5	1.5
Fe-Ni MANC	2.3	1.0	2.1	0.30	2.0	2.0	0.04	1.5	1.5

Total power loss is a sum of three components each given in a form of $kf^{\alpha}B^{\beta}$ where f is the frequency in kHz, B is the peak flux density in tesla, and k a proportionality constant.

Table II
Phase Relationship

N_S	N_R	A1	B1	C1	A2	A3	A4	Match?
12	8	0	300	240	180	0	180	Y
12	9	0	270	180	90	180	270	N
12	10	0	240	120	0	0	0	Y
12	11	0	210	60	270	180	90	N
12	12	0	180	0	180	0	180	N
12	13	0	150	300	90	180	270	N
12	14	0	120	240	0	0	0	Y
12	15	0	90	180	270	180	90	N
12	16	0	60	120	0	0	0	Y

Phase relationship (in degrees) for the flux linkage of coils with respect to Coil A1. For the combination of the N_S and N_R to work, the phases of intra-phase coils (A1 ~ A4) must match and inter-phase coils (A1, B1, C1) must be shifted by 120°. In some cases (N_R=8, e. g.), the phases may be brought into alignment by changing the individual coil's connection polarity (180° shift).

Table III
Torque Calculation

Method	Coil Current: 4 A	Coil Current: 8A
Arkkio's method	0.6054 Nm	1.2106 Nm
Integration of E-field	0.6038 Nm	1.2080 Nm
Time derivative of flux	0.6041 Nm	1.2081 Nm

Torque calculation by three methods. The torque is averaged over one electrical cycle.

Table IV
Design Parameters

No. of phase	**3**	
No. of rotor poles	14	
No. of stator slots	12	4 coils per phase
Stator radius	54 mm	
Rotor radius	32 mm	
Air gap	0.5 mm	
Active length	50 mm	
No. of turns	24	per coil, filling factor=0.6
Magnet remanence	0.4 T	
Voltage	246 V	amplitude
Torque	4.13 Nm	
Speed	6000 rpm	1.4 kHz electrical
Current	12 A (amplitude)	current density: 6.4 A/mm^2
Power	2.6 kW	output
Copper loss	29 W	
Iron loss (Temperature rise without active cooling)	93 W (230 °C)	3% silicon steel
	2.8 W (60 °C)	Fe-Ni MANC

Main design parameters and projected performance.

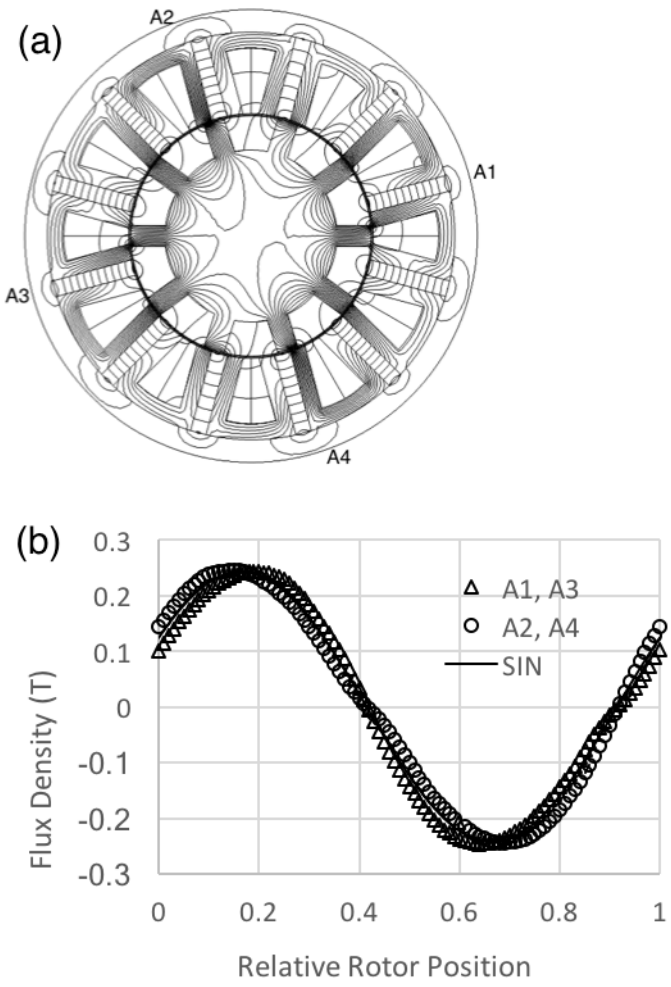

Fig. 1. (a) Flux lines for a flux switching permanent magnet motor. Twelve (12) coils are wound on a permanent magnet, magnetized tangentially without overlap and sharing a slot with adjacent coils. Magnet polarity alternates. The rotor has ten (10) poles. (b) Flux linkage for four coils (A1 and A2) in phase A. (Coils pairs A1/A3 and A2/A4 have the same linkage by symmetry.) Nearly sinusoidal profile is obtained by connecting the four coils in series.

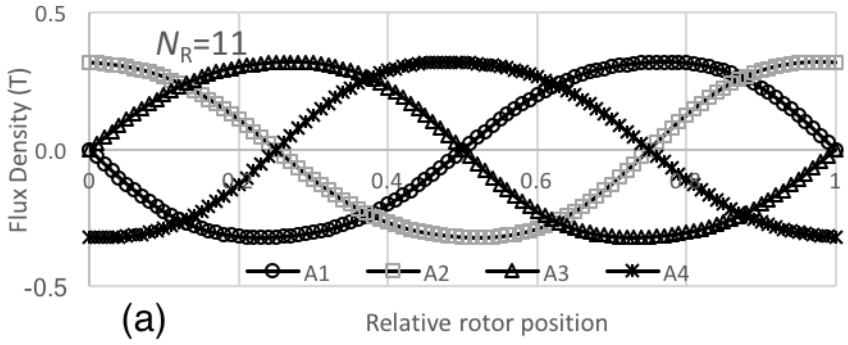

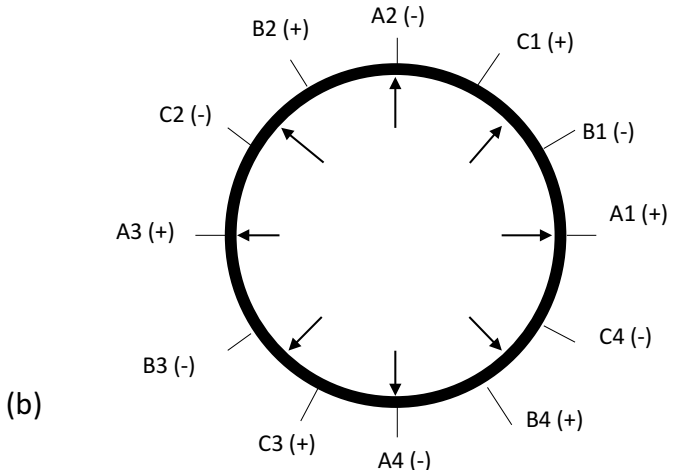

Fig. 2. (a) Flux linkage of four coils in one phase when the slot number (N_S) is 12 and the rotor pole number (N_R) is 11. The phases of these four coils are 90 degrees apart. (b) Relationship of coils (N_s=12) and rotor poles (N_R=8). As the rotor makes a mechanical rotation of 360/N_R degrees, each coil experience a full 360 degrees of electrical rotation. Note the polarity of the permanent magnet associated with each coil alternates as shown by + and – sign.

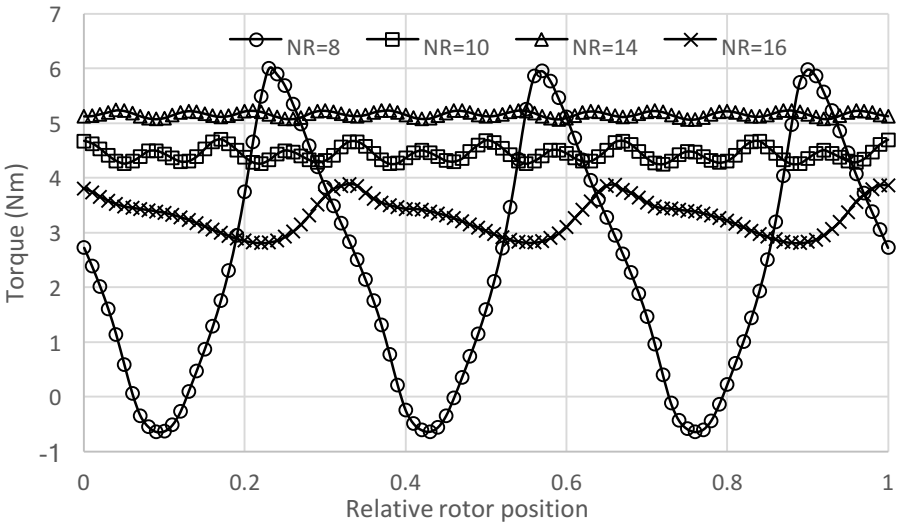

Fig. 3. Torque and ripple at I=15 A. The torque is higher with 14 poles than with 10 poles. The torque ripple also decreases. Much degraded performances are noted with 8- and 16-pole design. In all the cases, the number of stator slots (N_S) is set at 12.

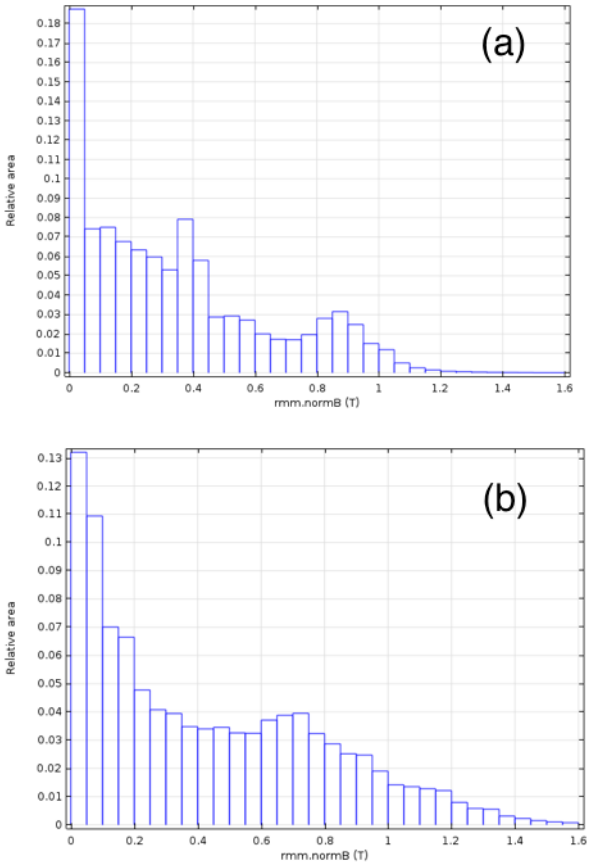

Fig. 4. Distribution of flux density (absolute value) in the soft-magnetic components. (a) no load, (b) full load.

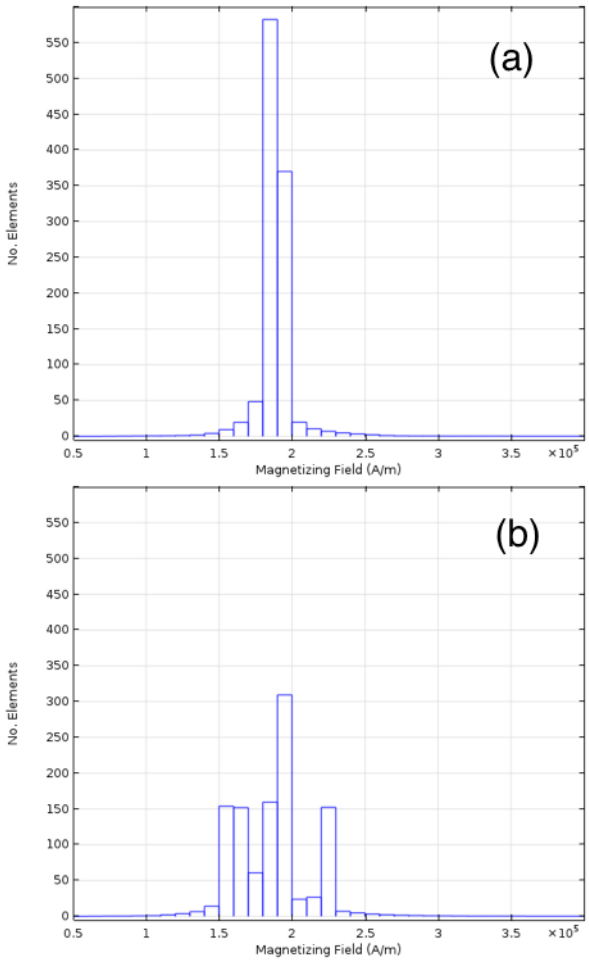

Fig. 5. Distribution of magnetizing field in the permanent magnets. (a) no load, (b) full load.